THE ASTROPHYSICAL JOURNAL, 307:698–710, 1986 August 15

SPECTRAL VARIABILITY OF CYGNUS X-2: STRUCTURE IN THE CIRCUMSOURCE MATERIAL

S. D. VRTILEK[1,2]
Columbia Astrophysics Laboratory, Columbia University
S. M. KAHN
Department of Physics, University of California at Berkeley
J. E. GRINDLAY
Harvard-Smithsonian Center for Astrophysics
D. J. HELFAND
Columbia Astrophysics Laboratory, Columbia University
AND
F. D. SEWARD
Harvard-Smithsonian Center for Astrophysics
Received 1985 August 27; accepted 1986 February 7

ABSTRACT

Cygnus X-2 was observed during 13 separate pointings in the course of 1 yr by the *Einstein* monitor proportional counter. During one of these pointings the objective grating spectrometer was also used. We find that the data from these observations are well fitted by single-component thermal bremsstrahlung models with temperatures ranging from 4–12 keV; however, two-component models, where one component is a blackbody, are not excluded. The X-ray light curve appears to be correlated with the 9.843 day optical period, possibly implying a partial eclipse of the X-ray source. During the high states there are irregular dips of up to 30% in intensity that last for 300–700 s. Our high spectral resolution grating data were taken during one of the high states when these dips occurred, and we are able to distinguish variable emission and absorption features due to Fe, O, and Ne. Our picture of Cygnus X-2 is consistent with an intrinsic thermal source surrounded by a hot accretion disk corona. We can use this model to explain the high and low X-ray states, the variability within the states, and the intensity dips which occur in the high states.

Subject headings: radiation mechanisms — stars: individual — X-rays: binaries

I. INTRODUCTION

Since its discovery in 1965 (Bowyer *et al.*) Cygnus X-2 has been one of the best studied of the Galactic X-ray binaries. The system consists of a $\sim 1.4\ M_\odot$ neutron star with a low-mass ($\sim 0.7\ M_\odot$) companion (Bradt and McClintock 1983; McClintock *et al.* 1984). Its optical counterpart V1341 Cyg (Giaconni *et al.* 1967) varies in spectral type from A5 to F2 (possibly due to X-ray heating) and has been shown to have an orbital period of 9.843 days (Cowley, Crampton, and Hutchings 1979; hereafter CCH). If V1341 Cyg fills its Roche lobe, as optical light variations imply it does, a distance of 8 kpc can be inferred. The fact that it took nearly 12 yr to establish an uncontested orbital period (CCH 1979; Chiappetti *et al.* 1983) and the controversy as to whether its compact companion is a white dwarf or a neutron star (Branduardi *et al.* 1980; McClintock *et al.* 1984) attest to the irregular temporal and spectral behavior of the source.

The X-ray intensity is thought to vary between two states (Bonnet-Bidaud and van der Klis 1982); modulation of the X-ray intensity at the 9.843 day period has been reported by Marshall and Watson (1979) and Ilovaisky *et al.* (1979) during the low state, although Holt *et al.* (1979) were unable to detect the period during a long-term observation. Erratic dips in intensity have been reported to occur only during the high state (Ilovaisky *et al.* 1979; Bonnet-Bidaud and van der Klis 1982). A weak X-ray burst was found by Kahn and Grindlay (1984).

In this paper we present X-ray spectroscopic observations obtained with the *Einstein* objective grating spectrometer (OGS) and the monitor proportional counter (MPC) instruments (§ II). The observations include data from both the "high" and "low" states of the source. The data from different states were studied separately (§ III); the spectra are well fitted by single-temperature thermal bremsstrahlung models with temperature varying with source strength. Our results are particularly interesting because our high-resolution soft X-ray (OGS) spectra, discussed in § IV, were taken during one of the high states when irregular dips occurred, and we are able to distinguish variable emission and absorption features due to Fe, O, and Ne during these states. Our observations are consistent with a picture of Cygnus X-2 as a soft thermal source with a hot accretion disk corona. In § V we discuss the implication of this model for the high and low X-ray states, the variability within the states, and the intensity dips which occur only in the high state. A comparison to other models proposed for Cygnus X-2 is also presented. The implications of the correlation found between the X-ray light curve and the 9.843 day optical period for X-ray heating of the companion star, and a partial eclipse of the X-ray source, are also discussed in § V.

[1] Now at NASA/Goddard Space Flight Center.
[2] NAS/NRC Research Associate.

II. OBSERVATIONS

The data consist of 13 observations made with the *Einstein* MPC. A total of 9.5×10^4 s of on-source data were processed. For one of these observations (1.5×10^4 s on-source), simultaneous coverage with the OGS was also obtained.

The MPC is described in detail by Gaillarditz *et al.* (1979) and by Grindlay *et al.* (1980). It was coaligned with the *Einstein* telescope to monitor sources which were being observed simultaneously by the focal plane instruments (Giacconi *et al.* 1979). The detector consisted of collimated proportional counters sensitive to X-rays in the range 1–20 keV. Eight-channel pulse-height spectra were accumulated by the MPC in 2.56 s bins. The estimated systematic errors in predicted background counts (Halpern 1984) are entirely negligible in comparison with the counts detected from Cyg X-2.

The characteristics and calibration of the OGS are described in detail by Seward *et al.* (1982) and by Kahn, Seward, and Chlebowski (1984, hereafter KSC). The instrument consisted of two gold bar transmission gratings, either of which could be inserted into the X-ray optical path at the exit from the *Einstein* mirror (Giacconi *et al.* 1979). The present observation used the 1000 lines mm^{-1} grating which has a spectral resolution of $E/\Delta E \approx 31E^{-1}$ (keV), as measured during pre-launch calibration. The dispersed spectra were projected onto the high resolution imager (HRI) (Henry *et al.* 1977). The OGS covered an energy range of 0.1–1.5 keV.

KSC conservatively estimated that the overall normalization of OGS spectra (with wavelength-dependent effective area determined from ground calibration of the telescope-grating–HRI combination and from observations of the Crab Nebula) is known to 50%. In order to improve this value we compared the normalizations of spectra fitted to simultaneous OGS and MPC data of objects (including the Crab Nebula) with well-determined and smooth spectral shapes over the energy range of overlap. Using this method we were able to determine that the OGS and MPC normalizations agree to within 10%. This result is model independent, applying equally for blackbody and thermal bremsstrahlung models for bulge sources and for a power-law model for the Crab. Since the relative normalization of the MPC is good to 5% for MPC channel 1, the region of overlap, and the absolute normalization of the higher MPC channels is known to 3%, we believe that our absolute OGS normalization is accurate to ~18%.

Table 1 lists the observations, the times they were taken, the effective exposure, and the phase of the observations relative to the 9.843 day orbital period (CCH 1979). Pointings range from 5 to 10 hr in duration (before removal of data gaps due to Earth occultations, South Atlantic Anomaly passage, and other causes). Figures 1*a*–1*d* show the MPC data for eight of the 13 observations. The long-term intensity variations of up to 50%, interpreted by Bonnet-Bidaud and van der Klis (1982) as being due to two intrinsic states of the source (high state, ~600–800 counts s^{-1}; low state, ~300–500 counts s^{-1}) are easily seen. One of the observations (not shown) has a count rate 50% higher (~1150 counts s^{-1}) than the nominal high state. Figures 1*a*, 1*b*, and 1*d* exhibit the short-term intensity dips which appear only when the intrinsic source is in the high state. The temporal behavior in the OGS (obtained by plotting the zero-order count rate as a function of time) shows several dips in the count rate coincident with those in the MPC data of Figure 1*b*.

A hardness ratio is plotted below each light curve in Figures 1*a*–1*d*. The qualitative results are independent of any detailed definition of the hardness ratio; we define it here as the ratio of the counts falling in the energy range 4–10 keV (MPC channels 4, 5, and 6) to those in the energy range 1–2 keV (MPC channels 1 and 2). The hardness ratios were computed for 40.96 s integration times. The correlation between the hardness ratio and the MPC count rate is shown in Figure 2. There is an overall increase in hardness ratio with decrease in count rate as expected for absorption; however, there is also concrete evidence for intrinsic source change since there is a large scatter in hardness ratios for any given intensity. An interpretation of the hardness ratio/count rate relationship is discussed in § V.

III. BROAD-BAND ANALYSIS

Inspection of the temporal behavior of the hardness ratio (Figs. 1*a*–1*d*) and of the hardness ratio versus intensity scatter plot (Fig. 2) suggests that a single spectral fit to all the data is

TABLE 1

LOG OF OBSERVATIONS

SEQUENCE NUMBER	UT TIME OF OBSERVATION			TIME ON-SOURCE (s)	BINARY PHASE RANGE[a]	COMMENT
	Year	Day	Seconds (start–stop)			
1626a	1978	338	28830.9–31698.1	1925.	0.66–0.67	
1626b	1978	339	30044.0–32337.8	2253.	0.76–0.77	
1626c	1978	344	19440.5–21693.3	2294.	0.25–0.26	
2747	1978	361	3000.2–4229.0	1229.	0.96–0.97	Intensity dips
2737	1978	361	19998.6–28026.7	4874.	0.98–0.99	
2753	1978	361	31426.4–74721.1	14665.	0.00–0.05	Intensity dips
824	1979	136	28292.1–64500.8	15158.	0.22–0.26	Intensity dips[b]
1626d	1979	152	80966.7–83342.4	2458.	0.90–0.91	
4338	1979	170	4914.3–22731.9	10370.	0.64–0.66	
4336	1979	170	22895.7–41368.7	11400.	0.66–0.68	
4339	1979	170	52755.5–68197.5	8070.	0.70–0.72	
4337	1979	170	68279.4–86383.7	10350.	0.72–0.74	
1626e	1979	177	33069.1–80214.1	9190.	0.39–0.44	Intensity dips

[a] Orbital phase is determined using JD = 2,442,659.722 for phase 0.0 and a period of 9.843 days from Cowley, Crampton, and Hutchings 1979, where phase 0.02 refers to superior conjunction of the optical star.

[b] OGS and MPC data taken simultaneously during this observation; MPC data only are analyzed for all other observations.

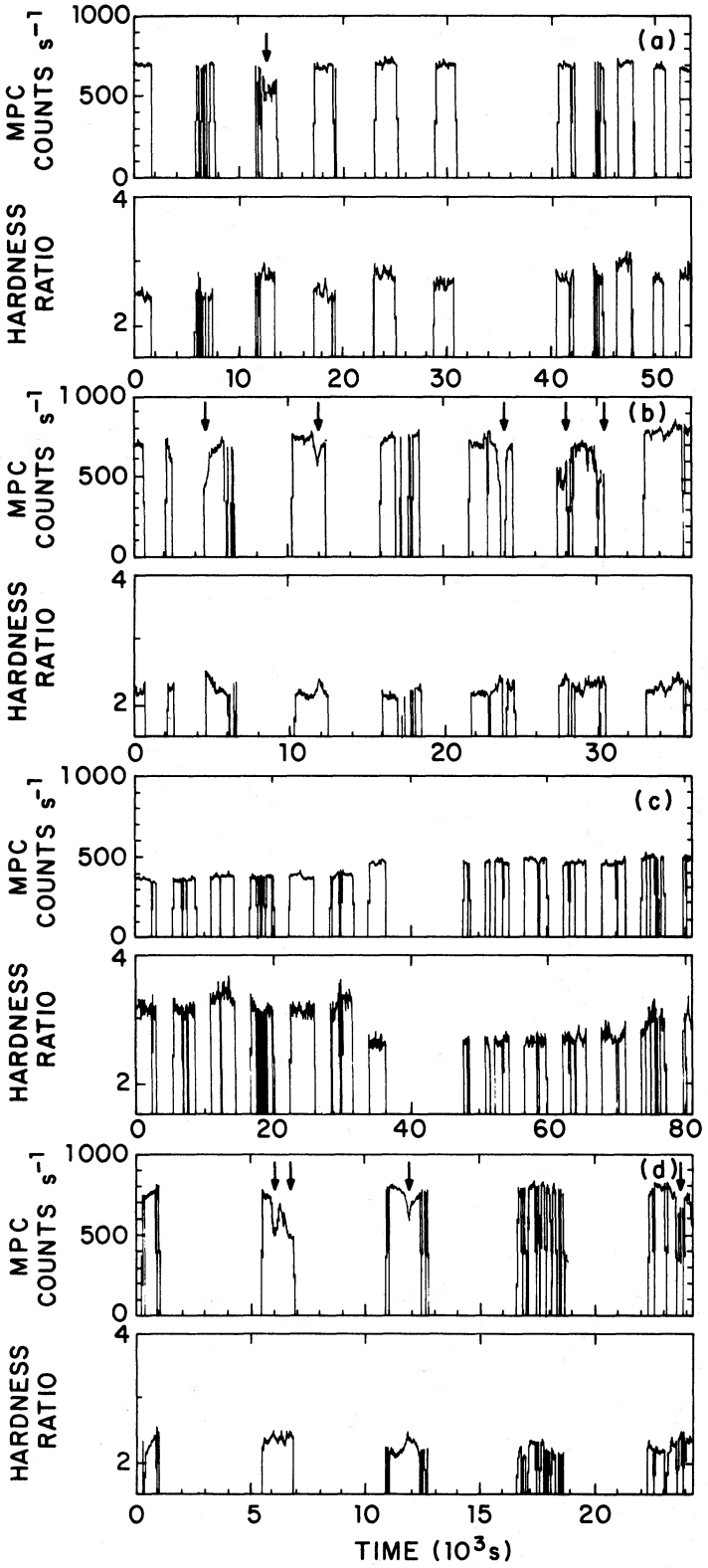

FIG. 1.—MPC total count rates and (4–10 keV/1–2 keV) hardness ratio vs. time. (*a*)–(*d*) Data continuous in time except for gaps due to Earth occultation, South Atlantic Anomaly passage, or telemetry dropouts. Since *Einstein* Observatory data are easily located by sequence numbers, these are given for reference here and elsewhere in this paper. (*a*) For sequences 2737 and 2753 observed 1978 December 27. The zero of the time axis corresponds to JD 2,443,870.2310 (binary phase 0.98). (*b*) For sequence 824 observed 1979 May 16. The zero of the time axis corresponds to JD 2,444,010.3275 (binary phase 0.22). (*c*) For sequences 4338, 4336, 4339, and 4337 taken on 1979 June 19. The zero of the time axis corresponds to JD 2,444,044.0569 (binary phase 0.64). (*d*) For sequence 1626e observed 1979 June 26. The zero of the time axis corresponds to JD 2,444,051.3827 (binary phase 0.39).

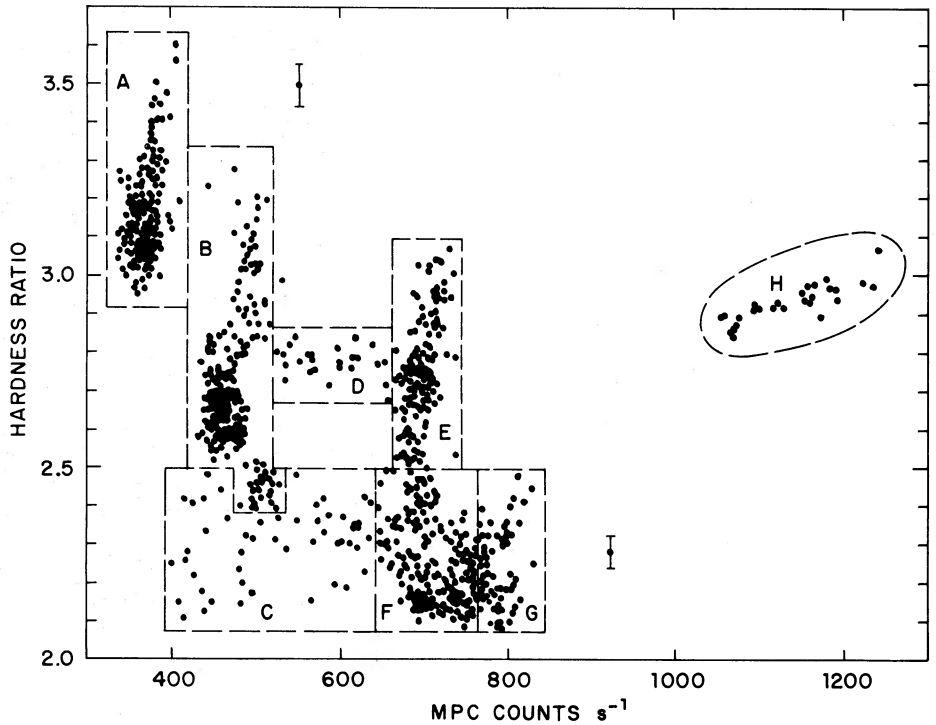

FIG. 2.—Correlation of (4–10 keV/1–2 keV) hardness ratio with total (1–20 keV) MPC count rates for all the data used in this study. Each point indicates a hardness ratio and count rate computed for a 81.92 s integration time. Typical 1 σ error bars are shown. The eight sections separated by dotted lines and labeled "A" through "H" represent the divisions within which spectral fits were attempted. Section C corresponds to dips in intensity from section F, and section D to dips from section E.

not practicable. To analyze the spectral behavior of Cygnus X-2, we divided the data into the eight sections, designated "A" through "H" in Figure 2. Since division of the data into fewer sections based solely on source intensity failed to give acceptable fits, a further subdivision including hardness ratio as an additional criterion was used. A single observation usually corresponds to a single such section, except where there are dips in that observation; the dips correspond to sections C and D. For sections C, F, and G we have OGS data in addition to the MPC data. The division described here is intended as a convenience in analysis only, not as a suggestion that the source actually has a corresponding number of discrete emitting states. The data presumably form a continuum; the divisions have been made such that data of the present quality cannot distinguish significant spectral differences within a division.

We have fitted power-law (PL), thermal bremsstrahlung (TB), single blackbody (BB), two-component blackbody (2BB), blackbody plus thermal bremsstrahlung (BB + TB), and power-law plus thermal bremsstrahlung (PL + TB) models to the data separately for each section shown in Figure 2. Since the MPC does not have sufficient resolution to detect the iron line between 6–7 keV reported by previous observers (Hasinger *et al.* 1985*a*; Hirano *et al.* 1984), we made no attempt to include a line in any of our models. Single-component thermal bremsstrahlung spectra with a Gaunt factor taken from Kellogg, Baldwin, and Koch (1975) gave the best fit in all cases. PL and BB models could be rejected. The two-component models all provided good fits, but there was no significant improvement in reduced χ^2 (Table 2). Accordingly, although we cannot exclude two-component models, the addition of a second component is not justified on the basis of the present data. White *et al.* (1985) have found that their data on Serpens X-1 and XB 1728−337 allowed a similar indeterminacy in the form of the continuum model. The best-fit spectral parameters obtained for TB models are listed in Table 3. A comparison to other models is presented in § V.

Surprisingly, the lowest intensity states have the highest temperatures and the least column density (see Table 3). The column density for state A is at the limit of detectability of the MPC, which cannot distinguish column densities less than 3×10^{21} cm^{-2} (Halpern 1984). Since the neutral hydrogen column density due to the intervening interstellar material to Cygnus X-2 is determined to be 2.3×10^{21} cm^{-2} from the relationship between interstellar reddening and X-ray absorption (Ryter, Cesarsky, and Adouze 1975; Gorenstein 1975), we can conclude that the low-intensity state is not due to obscuring material which covers the intrinsic source, but that it is due to a change in the source itself.

In state B the hardness ratio is mostly lower than in state A, although there is some overlap, and the intensity is ~30% greater. The column density in state B is distinctly higher than that for intervening interstellar material, indicating that there is obscuring material in the line of sight. However, the normalizations are also lower than during the high states (E–H), possibly indicating that some of the flux has been Compton scattered out of the line of sight by a highly ionized obscuring component.

States C, F, and G occur during one of the high-intensity states of Cygnus X-2, with C corresponding to the dips pointed out in Figures 1*b* and 2. For these states we have data from both the OGS and the MPC. The best fit to state G for the MPC and OGS combined is shown in Figure 3*b*. Where data from both instruments are available, fits to the MPC data alone (Fig. 3*c*) fall below the data from the low-energy OGS

TABLE 2

CYGNUS X-2 SPECTRAL PARAMETERS

State	Sequence Number	Average[a] (counts s^{-1})	A_{TB} (cm^{-2} s^{-1} keV^{-1})	kT (keV)	N_H (10^{21} cm^{-2})	Instruments
A low	4338	347	0.52	12.66 (+1.87 −1.58)	0.82 (+1.42 −0.32)	MPC
	4336	379	0.58	12.48 (+2.12 −1.54)	1.74 (+1.49 −1.27)	MPC
B medium	4339	452	1.14	7.01 (+0.53 −0.48)	3.54 (+1.27 −1.25)	MPC
B medium	4337	483	1.01	8.73 (+0.85 −0.71)	3.81 (+1.23 −1.46)	MPC
B medium	1626a	503	1.22	7.18 (+0.57 −0.50)	2.29 (+1.22 −1.20)	MPC
C dips	824	518	2.11	4.63 (+0.19 −0.17)	5.99 (+0.63 −1.32)	MPC
			1.96	4.61 ± 0.4	3.55 ± 0.2	MPC + OGS
			1.85	3.57	3.71	OGS
D dips	2747, 2753	562	2.07	5.19 (+0.19 −0.19)	7.97 (+0.55 −0.39)	MPC
C dips	1626e	591	2.41	4.63 (+0.17 −0.14)	6.12 (+0.07 −1.33)	MPC
E high	2737	698	2.70	5.87 (+0.24 −0.24)	6.71 (+1.05 −0.91)	MPC
	2753	697	2.35	5.54 (+0.31 −0.30)	6.77 (+0.99 −1.02)	MPC
F high	824	741	3.13	4.44 (+0.19 −0.19)	5.27 (+0.93 −1.00)	MPC
			2.92 ± 0.3	4.65 ± 0.3	2.51 ± 0.4	MPC + OGS
			2.91	3.43	2.67	OGS
F high	1626d	740	2.99	4.60 (+0.20 −0.20)	5.17 (+1.14 −0.90)	MPC
G high	1626e	772	3.17	4.55 (+0.19 −0.19)	5.25 (+1.06 −0.91)	MPC
G high	824	775	3.11	4.65 (+0.20 −0.23)	5.43 (+0.88 −0.70)	MPC
			2.95 ± 0.4	4.57 ± 0.3	3.16 ± 0.3	MPC + OGS
H high			3.24	3.63	3.09	OGS
	1626c	1140	3.49	6.11 (+0.43 −0.36)	7.35 (+1.24 −1.27)	MPC

NOTE.—Assumed spectral model has the form $N(E) = A_{TB}e^{-E/kT}e^{-N_H\sigma(E)}g(E; kT)$. The effective absorption cross section $\sigma(E)$ was calculated on the assumption of neutral cosmic-abundance material (Morrison and McCammon 1983); $g(E; kT)$ is the Gaunt factor as given by Kellogg, Baldwin, and Koch 1975.

[a] MPC channels 1–7.

TABLE 3

DISCRETE FEATURES IN THE CYGNUS X-2 HIGH STATE SPECTRA

Wavelength (Å)	Comment	Possible Identification	EW (Å)	State
11.1 ± 0.3.....	Emission complex	Fe XVII, Fe XXIII–XXIV	0.05 ± 0.02	F (high)
11.7 ± 0.2.....	Emission complex	Fe XXII–XXIII	0.09 ± 0.03	F (high)
12.3 ± 0.4.....	Emission complex	Fe XXI, Ne X	0.15 ± 0.15	G (high)
12.9 ± 0.4.....	Emission complex	Fe XX, Ni XX	0.16 ± 0.05	F (high)
13.7 ± 0.4.....	Emission complex	Fe XVII, Ne IX, Ne VIII	0.14 ± 0.05	G (high)
14.3 ± 0.2.....	Absorption complex	Fe XVIII	0.19 ± 0.07	E (dips)
14.3 ± 0.2.....	Absorption line	Fe XVIII	0.09 ± 0.03	G (high)
16.1 ± 0.2.....	Emission complex	O VIII, Fe XVIII	0.13 ± 0.04	F (high)
16.5 ± 0.3.....	Emission complex	Fe XVII	0.13 ± 0.04	G (high)
16.7 ± 0.4.....	Emission complex	Fe XVII	0.10 ± 0.03	F (high)
19.7 ± 0.4.....	Emission complex	?	0.21 ± 0.06	G (high)

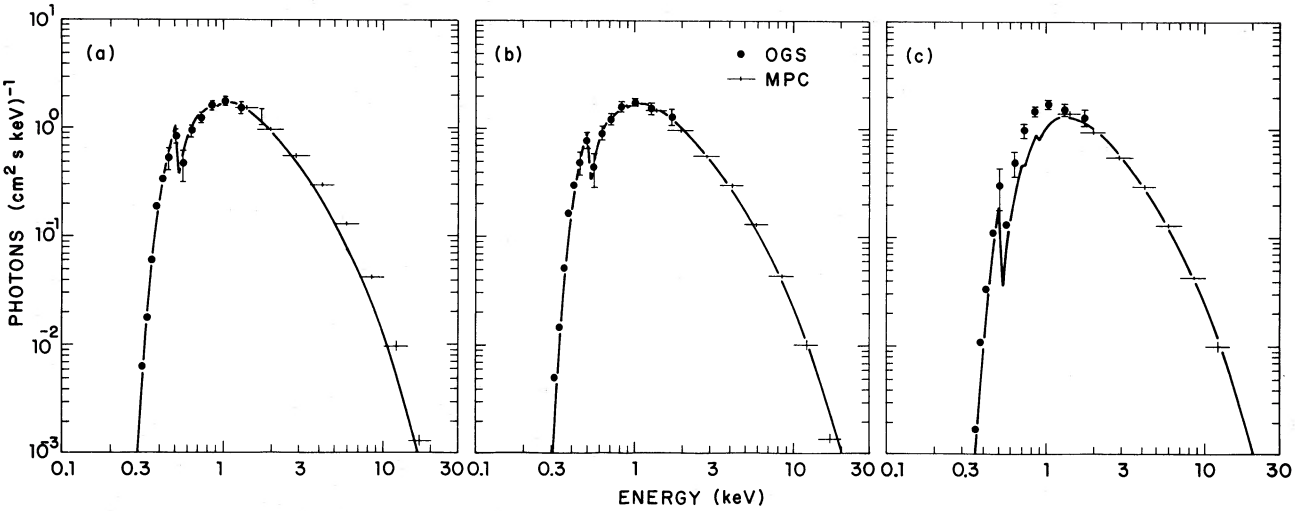

FIG. 3.—(*a*) Best-fit TB model to the OGS spectrum for state G of Fig. 2 extrapolated to 20 keV. (*b*) Best-fit TB model to the spectrum for state G when the MPC and OGS are combined. Each OGS point shown represents seven resolution elements; the bars indicate 1 σ errors. Channel boundaries and 1 σ errors are indicated for the MPC channels by the widths and heights of the crosses, respectively. (*c*) Best-fit TB model to the MPC spectrum for state G of Fig. 2 extrapolated to 0.3 keV.

channels, due to an overestimate of the column density. We also find that the OGS data fitted alone (Fig. 3*a*) underestimate the temperature. We modified the nonlinear least-squares model-fitting program used by KSC for their OGS analysis to provide a variance-covariance matrix of the model parameters that can be used to determine the correlation between the parameters. This technique shows the expected high correlation between the temperature and normalization when the OGS data are used alone. We find that fitting the MPC and OGS together greatly reduces this correlation, resulting in a more reliable determination of the model parameters. The joint MPC and OGS fit is thus very important for a reliable determination of the spectrum.

We find that Cygnus X-2 in its high state is well fitted by a single thermal bremsstrahlung spectrum from 0.3–20 keV. During both the dip and nondip states the neutral oxygen edge (0.533 keV) is clearly seen. The oxygen edge is more prominent in the deconvolved spectra than in the raw count spectra (shown below), partly because the deconvolved spectra are background subtracted and also because the OGS efficiency is very small near the oxygen edge so that slight effects are somewhat enhanced in the deconvolved spectra. During the dip state the column density increases; again the normalization also decreases, indicating that photoelectric absorption alone does not account for the decrease in intensity during the dips. There is also slight evidence for an absorption feature at 2–3 keV. Such a feature was noted by Branduardi *et al.* (1984), and attributed to K-shell absorption by Mg and Si hydrogen- and helium-like ions. Finally, for state G (for sequence 824 this is seen in the last satellite orbit of Fig. 1*b*) and state H, where the hardness ratio is positively correlated with intensity instead of the "normal" inverse correlation expected for absorption, we find a column density comparable to that of the dip state. For these states the column densities increase with increasing intensity. A possible explanation of this behavior is discussed in § V.

IV. EMISSION AND ABSORPTION FEATURES

The high-resolution (OGS) observations are plotted at full resolution for the states C (dips), F (high), and G (high) in Figures 4*a*, 5*a*, and 6*a*. Here the data are raw counts per 0.4 Å bin, uncorrected for spectral response, background, or higher order contributions. The error can therefore be taken as the square root of the detected number of counts in each bin. The method for extracting the dispersed spectra is described in detail by KSC. Since the emission and absorption features are weak and superposed on a strong, highly sloping continuum, it is necessary to subtract the continuum from the raw count spectra in order to isolate the features. As described in § III, the best-fit model parameters are obtained by combining MPC and OGS data. Since there is a 10% uncertainty in the relative normalization of the instruments, for the purpose of determining the continuum in the OGS we used only the temperature and column density from the combined fit and the normalization that best fits the OGS data alone. The residuals are plotted in Figures 4*b*, 5*b*, and 6*b*, with errors determined from counting statistics alone since these dominate the uncertainties of baseline determination. Emission and absorption features of greater than 3 σ significance were selected and are listed with their equivalent widths and possible identifications in Table 4. The nondip spectra clearly exhibit emission lines, whereas in the dip spectrum (Fig. 4) there is evidence for an absorption feature at 14.3 Å. To check if the absorption feature is due to a line or an edge, fits were made to a continuum plus Gaussian line and continuum plus absorption edge. The best fit was found to be a continuum plus Gaussian line (plotted on Fig. 4*a* as a dotted line), and indeed the width of the feature is much too small for an edge. The 14.3 Å feature is thus attributed to Fe XVIII, rather than to the O VIII edge. There is also evidence for an absorption feature at 14.3 Å during the nondip state G. The presence of this feature is consistent with an interpretation

TABLE 4

REDUCED χ^2 VERSUS MODEL

	MODEL			
STATE	TB	BB + TB	BB + BB	PL + TB
High (G).....	1.6	1.3	1.7	1.8
Dips (C).....	1.3	1.4	1.5	1.7

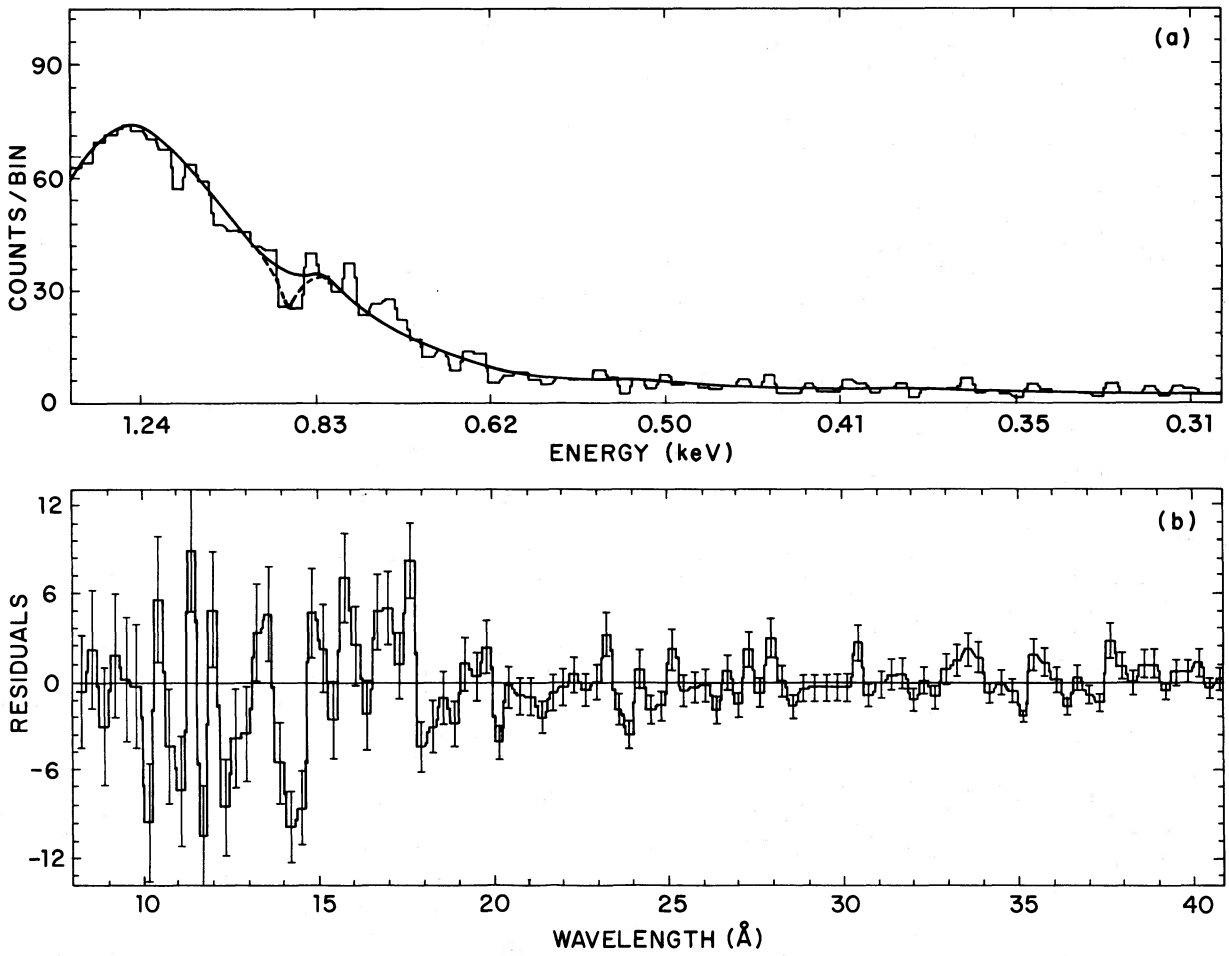

FIG. 4.—(*a*) OGS raw count spectrum of Cygnus X-2 during the dips of the high state (state C of Fig. 2). Data are counts per 0.4 Å bin. Solid line represents the best-fit TB continuum spectrum. Dotted line is the best fit with a continuum plus Gaussian line. (*b*) Residuals after subtraction of the continuum from the raw counts in (*a*). Error bars shown are for 1 σ count statistics only.

of the dips as being caused by clumps of accreting matter, and with state G being due to a higher accretion rate as discussed in § V below; in both cases there is more accreting matter in the line of sight causing the absorption. The emission lines ascribed to Fe XXII–XXIII around 11.7 Å and those ascribed to Fe XVII around 16.5 Å are quite prominent; indeed they are the strongest ones expected for a low-density, hot collisional plasma with $T > 5 \times 10^6$ K (Doschek and Cowan 1984). If the lines are due to photoionized material, then much lower temperatures would be appropriate. In general, the density of possible features in the region from 10–18 Å is very high, so the identifications must be considered tentative.

We found no evidence for anomalous abundance of oxygen and nitrogen in the absorbing matter as found for Sco X-1 by KSC and by Brinkman *et al.* (1984). The calculations of Iben and Tutukov (1984) for the evolution of low-mass close binaries suggest the possibility of an excess in the nitrogen-to-carbon abundance ratio. Chiappetti *et al.* (1983) found evidence that carbon is underabundant with respect to nitrogen in their analysis of the *IUE* spectra of Cygnus X-2. We thus attempted a fit in which the nitrogen and carbon abundances were varied with oxygen held at its cosmic value but were unable to confirm any abundance anomalies. The 3 σ (99.9% confidence level) upper limit to any anomalous abundances of oxygen, nitrogen, or carbon is a factor of 2.

V. DISCUSSION

a) Comparison to Other Models

Previous broad-band X-ray spectral studies of Cygnus X-2 are consistent with (1) a single-temperature thermal bremsstrahlung model with temperatures varying from 3 to 7 keV as used by Pravdo (1983) for *HEAO 1* A-2 observations; (2) a power-law spectrum below 2 keV plus thermal bremsstrahlung at higher energies used by Branduardi-Raymont, Chiappetti, and Ercon (1984) for *Ariel 5* observations; (3) a four-component model, consisting of a blackbody from the neutron star Comptonized by a stellar corona and a multitemperature blackbody from the disk Comptonized by an accretion disk corona used by Hirano *et al.* (1984) for their *Hakucho* observations; (4) 2 keV blackbody plus 5–15 keV thermal bremsstrahlung spectra used by Swank and Serlemitsos (1985) for *OSO 8* data on bulge sources of the Sco X-1 type. A $\sim$2 keV blackbody plus a 8–13 keV thermal bremsstrahlung and a 1.2 keV blackbody plus a 7 keV thermal bremsstrahlung have been reported by Hasinger *et al.* (1985*a*, *b*) for their *EXOSAT* observations of Cygnus X-2.

In Table 2, we list the reduced χ^2 during the high and dip states for each of these models: pure thermal bremsstrahlung, thermal bremsstrahlung plus blackbody, power-law plus thermal bremsstrahlung, and two blackbodies. Examples of the

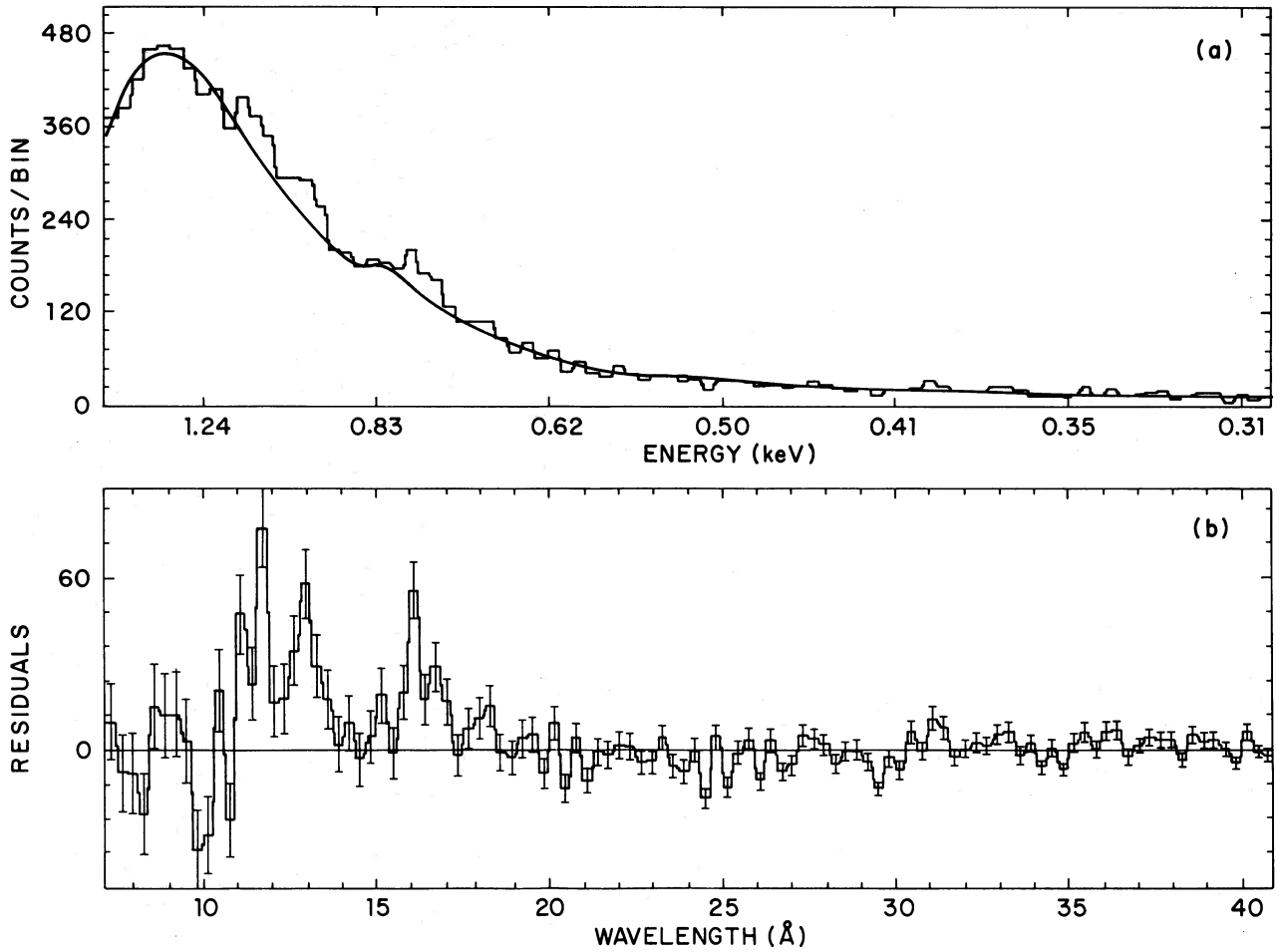

FIG. 5.—(*a*) OGS raw count spectrum of Cygnus X-2 during the high state (state F of Fig. 2). Data are counts per 0.4 Å bin. Solid line represents the best fit continuum spectrum. (*b*) Residuals from subtraction of the continuum from the raw counts in (*a*). Error bars shown are for 1 σ count statistics only.

two component models, which also give fits of acceptable χ^2, are shown in Figures 7*a*, 7*b*, and 7*c*.

We obtain good fits to single-temperature TB in agreement with Pravdo. We note that whereas Pravdo required the relative normalizations between two detectors on *HEAO 1* to be a free parameter, we required no such adjustment to the normalizations of the OGS and MPC; the calibration of the two instruments was held fixed. Pravdo's model (1983) for the Cyg X-2 binary system, a Comptonized X-ray cloud around a neutron star, can also be used to explain our observations.

We are able to obtain acceptable fits (reduced $\chi^2 = 1.8$) to a combined power law plus thermal bremsstrahlung, but the detailed behavior of the PL and TB components are quite different from that observed by Branduardi-Raymont, Chiappetti, and Ercon.

A simplified version of the Hirano *et al.* model (two blackbodies) also fits our data well in the high states and in the dip state. Since our low-state data are restricted to MPC observations, we do not have enough degrees of freedom to attempt a fit to the more complicated, multitemperature model. If we accept the simple two blackbody model, then with a distance to the source of ~ 8 kpc, the radii of the emitting regions for the blackbodies are ~ 9 km for the neutron star component (1.6 keV), and ~ 90 km for the disk component (0.5 keV BB) during the high state, and ~ 8 and ~ 70 km during the dips. The reduction in the emitting area of the softer blackbody then accounts for the presence of the dips. This is in disagreement with Hirano *et al.*, who find that their *soft* component remains steady and their hard component varies to give the different states.

Our high-state data can also be fitted to a blackbody plus thermal bremsstrahlung model. The blackbody component is again of a temperature (1.6 keV) and size (6 km) that may be associated with emission from a neutron star.

We do not find that subtracting the low or dip states from the high state results in a 2 keV blackbody attributable to emission from the neutron star as found by Makishima and Mitsuda (1985) for four other galactic bulge sources. This could simply mean that during our observations the flux from the neutron star is never completely obscured.

Recently the validity of the two-component models for low-mass X-ray binaries (LMXBs), in which one component (usually a blackbody) is attributed to direct emission from the neutron star, has come into question; Lewin and van Paradijs (1985) point out that LMXBs with *evolved* companions are likely to have fairly strong magnetic fields ($\sim 10^{10}$ G), which in turn indicates that the inner part of the accretion disk will terminate at the magnetosphere and not on the surface of the neutron star. CCH have shown that V1341 Cyg, the companion star to Cygnus X-2, is an evolved F star. Hasinger *et al.*

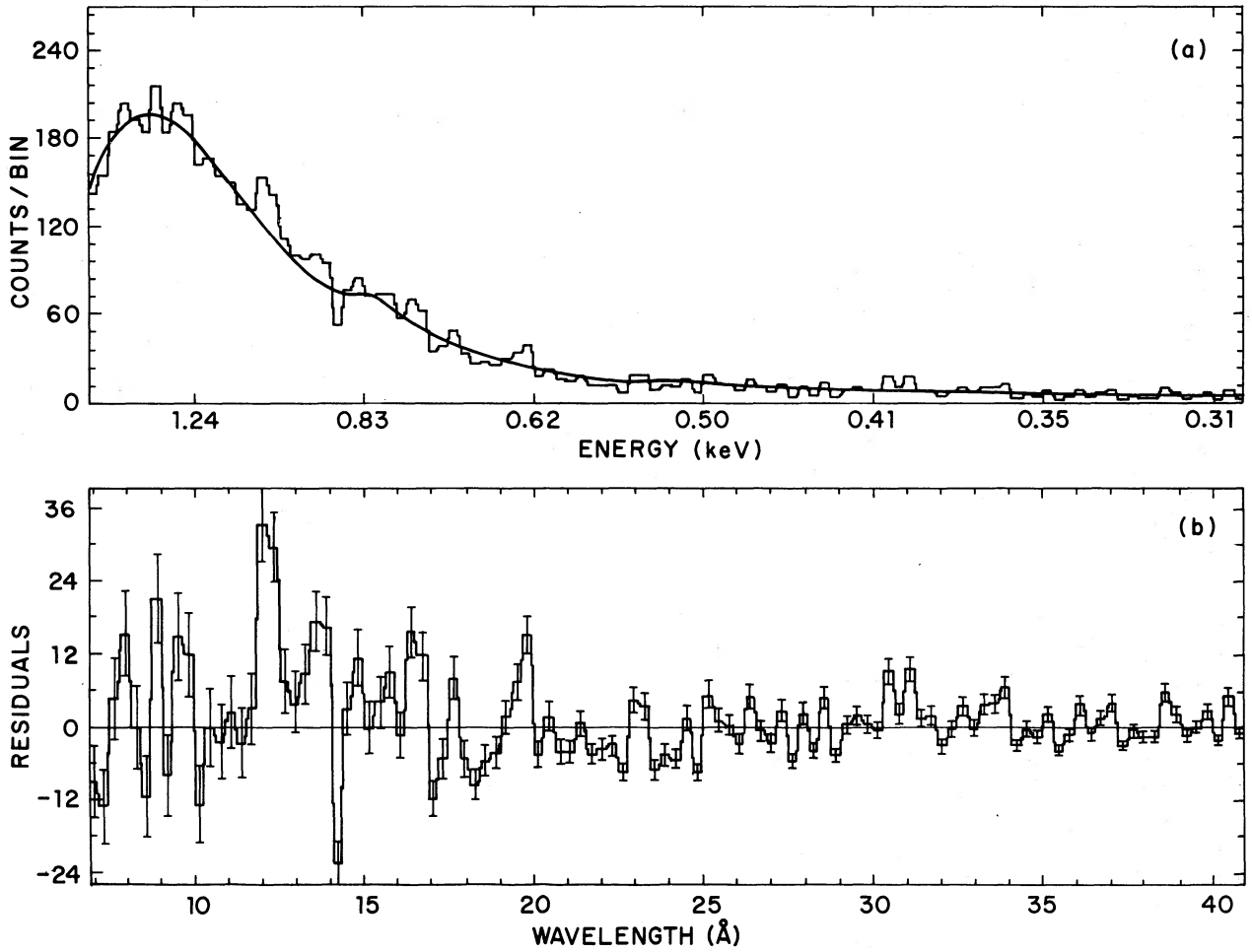

FIG. 6.—(*a*) OGS raw count spectrum of Cygnus X-2 during the last satellite orbit of Fig. 1*b* (state G of Fig. 2). Data are counts per 0.4 Å bin. Solid line represents the best-fit continuum spectrum. (*b*) Residuals after subtraction of the continuum from the raw counts in (*a*). Error bars shown are for 1 σ count statistics only.

(1985*b*) have reported quasi-periodic oscillations from Cygnus X-2 which imply a magnetic field of 5×10^{10} G with a corresponding magnetospheric radius of 150 km.

b) The High/Low States

The large-scale fluctuations in X-ray intensity appear to be correlated with the 9.843 day optical orbital period determined by CCH. The binary phase coverage and extrapolated X-ray light curve are shown in Figure 8. We follow the phase convention of CCH with phase zero very nearly the time of conjunction with the X-ray source in front.

To check for a correlation between the X-ray and optical fluxes we computed linear correlation coefficients between the X-ray light curve and each of the four light curves reported by CCH: a *V*-band light curve for all of their data; a *V*-band light curve excluding flares; a *U*-band light curve for all their data; and a *U*-band light curve for data before JD 2,442,520. (CCH note that the source underwent a change at this date, showing a 0.11 mag increase in optical brightness and a factor of 2 decrease in X-ray intensity. The source reverted to its former state shortly afterward.) Our observations were taken $\sim$4 yr after CCH, so that our phases may be shifted by up to $\sim$0.1 cycle from theirs due to uncertainty in the ephemeris. However, since all our observations are close together in time, the relative phase shifts are very small, and therefore the correlation analysis is justified. The highest correlation coefficient (0.67) was found between the X-ray curve and the *U*-band curve before JD 2,442,520. Since the number of points (15) used to determine the coefficient is so low, we used Efron's (1982) bootstrap method to place confidence limits on the correlation coefficient. One thousand trials were run for each case, giving $0.67^{+0.08}_{-0.12}$ (1 σ) for the X-ray to *U*-band correlation coefficient which corresponds to a confidence level of $\sim$97%–99.9%. No significant correlations occur in the other cases. The possibility of this correlation was predicted by CCH, since the changes they observed in spectral type with orbital phase were interpreted as an indication that V1341 Cyg is being heated by the incident X-radiation from Cyg X-2, in a way similar to the heating of HZ Her by Her X-1.

The binary-phase dependence of the correlation between X-ray and optical luminosity implies that the X-ray low state of Cygnus X-2 is due to a partial eclipse of the emission region. At binary phases where we see both an unobstructed X-ray source and the X-ray heated side of the companion star, both X-ray and optical fluxes are high; around binary phase 0.6 the X-ray source is partially eclipsed, and we see the unheated side of the companion, giving low X-ray and optical fluxes.

In Figure 9 we have redrawn the schematic diagram of Cygnus X-2 shown by CCH (1979), marking the binary phases for the following: the high states (E, F, G, H), the short-term

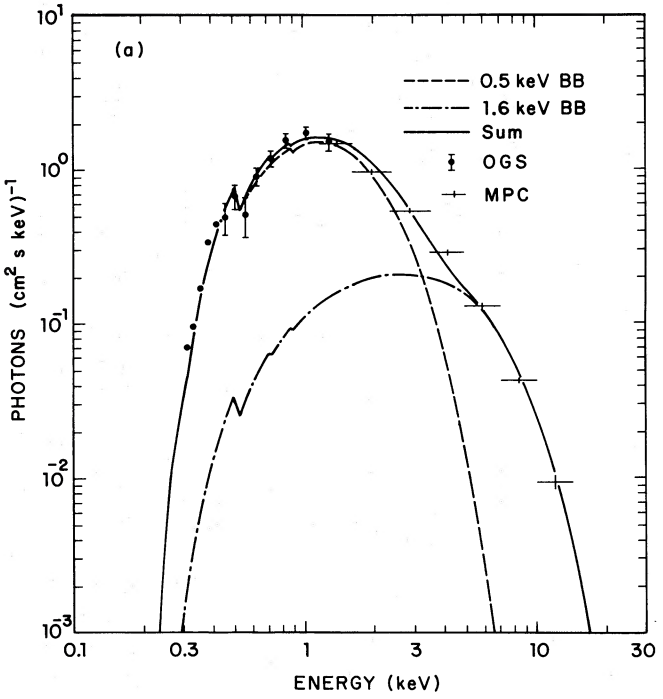

FIG. 7a

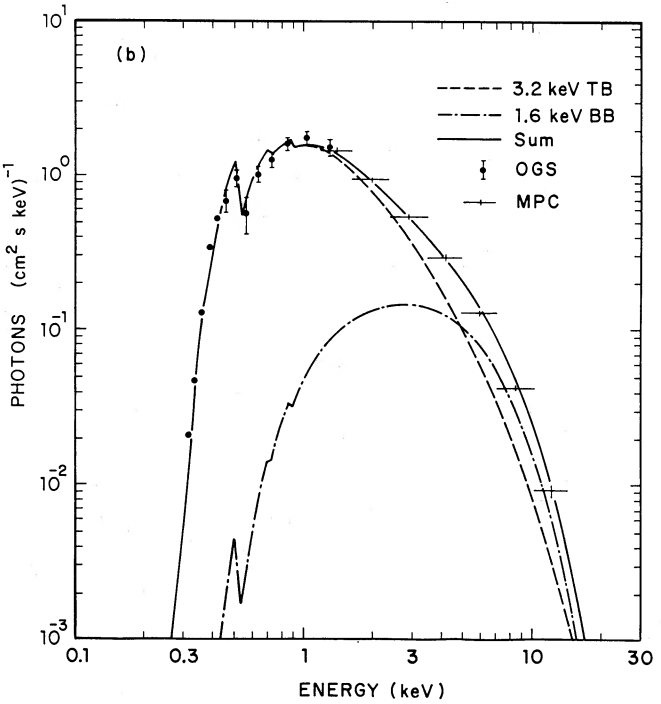

FIG. 7b

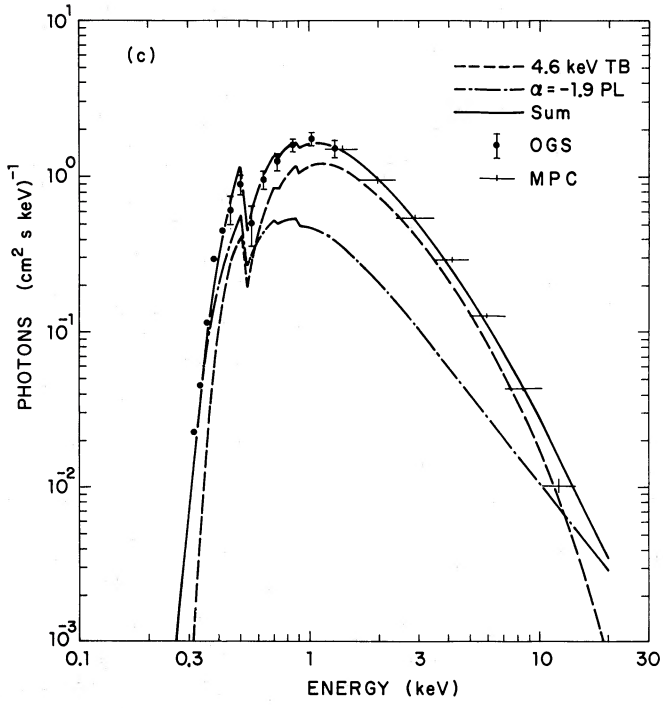

FIG. 7c

FIG. 7.—Best fit to state G of Fig. 2, using MPC and OGS data combined, for (*a*) 2BB; (*b*) BB + TB; (*c*) PL + TB.

intensity dips (C, D), the low states that show evidence for absorption (B), and the low states which show no absorption but very high temperatures (A). During the high state the X-ray source is unobscured except by the accretion stream, which may include uneven lumps that could lead to the absorption dips. If we attribute the low state with high temperatures to Comptonization in a hot corona, then during phase ~0.64–0.69 the accretion disk must be oriented so as to obscure the X-ray source but not the hot corona. The low state with some absorption (B) then may be caused by partial obscuration of both the X-ray source and the corona.

If we interpret the lowest state (A) to be due to the hot corona alone, then we can use the temperature of this state to estimate the size of the coronal region; following White and Holt (1982),

$$R_c = (M_x/M_\odot)(T_c/10^7)^{-1}\, R_\odot,$$

where M_x designates the mass of the accreting X-ray source and T_c the coronal temperature in Kelvins. This gives us a coronal radius of $\sim 0.1\, R_\odot$. Using a binary separation for the system of $\sim 26\, R_\odot$ as given by CCH and their neutron star to optical companion mass ratio of 2.2, we obtain an outer radius for the disk of $3.2\, R_\odot$, using Table 2 of Lubow and Shu (1976). The relative size of the disk is shown in Figure 9.

c) The Luminosity/Spectral Temperature Relation

The behavior shown in Figure 2 is markedly different from that reported by Branduardi *et al.* (1980) for their luminosity/spectral temperature correlation. The correlation they observed showed a double-valued relation between intensity and hardness ratio, similar to the theoretical prediction by Kylafis and Lamb (1982) for the behavior of X-ray emission from an accreting degenerate dwarf, which led to their suggestion that Cygnus X-2 is a white dwarf. However, Kylafis and Lamb also predicted an absolute upper limit to the X-ray luminosity of a degenerate dwarf which is far below the X-ray luminosity deduced for Cygnus X-2 by observations since. In particular, if the luminosity observed for Cygnus X-2 is attributed to a white dwarf, then the distance to Cygnus X-2 would have to be less than 300 pc, whereas the optical study of McClintock *et al.* (1984) showed that it must be at a distance greater than 1100 pc.

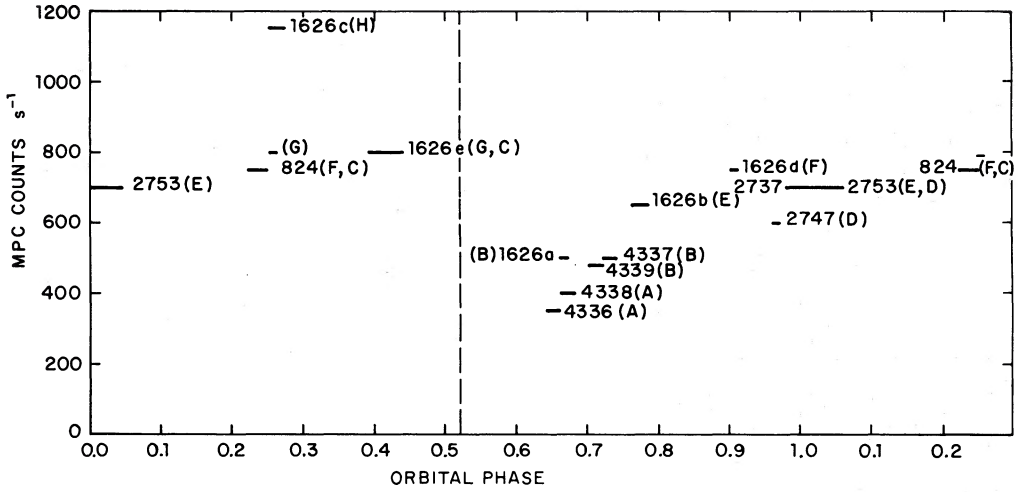

FIG. 8.—*Einstein* MPC count rates, summed over all channels and averaged over each observation, shown as a function of 9.843 day orbital phase (as defined by CCH), for all of the sequences used in this study. Length of horizontal bar, numbered according to sequence, indicates the duration of the observation. Dashed line at $\phi = 0.52$ indicates where X-ray eclipses would occur for a suitable orbit inclination. Sequence numbers are shown for reference (see Table 1).

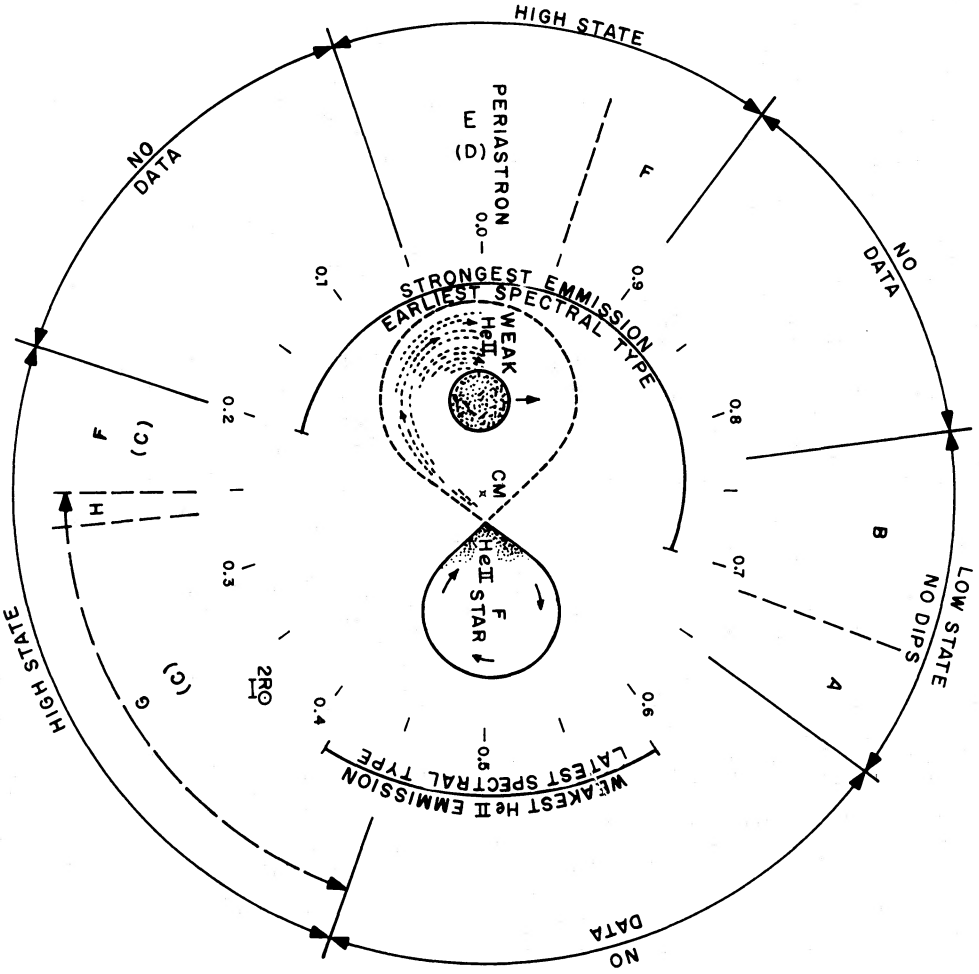

FIG. 9.—Schematic diagram of the Cyg X-2 system seen pole-on, redrawn from CCH Fig. 5 (with permission from A. Cowley). We have designated the location of our high states (with dip states in parentheses), the low states with absorption, and the low states with no absorption but very high temperatures.

Our results *are* consistent with those of Makishima and Mitsuda (1985), who also find a positive correlation between luminosity and hardness ratio for high-luminosity ($L_x > 5 \times 10^{37}$ ergs s^{-1}) galactic bulge sources (not including Cygnus X-2). The correlation is less well defined for lower luminosity sources ($10^{37} \geq L_x \geq 5 \times 10^{37}$ ergs s^{-1}), and becomes negative for very low luminosities ($< 10^{37}$ ergs s^{-1}). In the case of Cygnus X-2 we find that this luminosity/hardness ratio behavior occurs for high and low luminosity states of the same source. During our observations, the 2–10 keV luminosity of Cygnus X-2 varied from $\sim 3 \times 10^{37}$ ergs s^{-1} (A) to $\sim 2 \times 10^{38}$ ergs s^{-1} (H). We attribute the simultaneous increase in column density and intensity during the highest states to an increase in the accretion rate; the accreting matter which causes the higher intensity also causes the obscuration.

d) The Absorption Dips

We assume that the absorption dips (states C and D) are likely to be caused by clumps of accreting matter that intersect the line of sight. The dips appear to be independent of each other: that is, the size and shape of each dip is different from the one preceding or following it, as one would expect from random clumps. This is consistent with the observed increase in column density and the presence of an absorption line in the high resolution data during the dips. However, we note that in all cases a decrease in normalization accompanies the dips.

A possible explanation for the reduction in normalization could be that the blobs causing the obscuration are dense in the center and thin out at the edges. Then the reduction in normalization could be due to part of the source of photons being completely blocked out by the thick region, with the increase in column density caused by the thin outer regions that only partially obscure the source. This explanation requires the X-ray emitting area to be extended, as is consistent with our suggestion of an extended hot corona around the central source.

An alternate explanation of the decrease in normalization is to assume that the obscuring material is highly ionized. In that case, Compton scattering may provide some opacity along the line of sight in addition to photoelectric absorption. Since the Compton cross section is essentially independent of energy, a nonzero Compton depth will appear as an overall decrease in normalization. The observed decrease is consistent with Compton depths ranging from 0.0 to a maximum of 0.3. A typical Compton depth of 0.15 implies an obscuring column density of $\sim 2 \times 10^{23}$ cm^{-2}. The column density associated with purely neutral absorbers is $\sim 2 \times 10^{21}$ cm^{-2}; hence, the heavy elements may be as much as 99% ionized.

Such a high degree of ionization can result from photoionization by the central X-ray source itself. As shown by Hatchett, Buff, and McCray (1976), the state of the gas in such an environment is essentially controlled by the ionization parameter $\xi = L/nD^2$, where L is the total ionizing luminosity, n is the electron density, and D is the distance from the X-ray source. Using the results of Kallman and McCray (1982) for the model closest to our situation, we find that in order for the gas to be 99% ionized in the principal absorbing metal, oxygen, we require ξ of ~ 250 ergs cm s^{-1}. Using our measured luminosity of $\sim 5 \times 10^{37}$ ergs s^{-1} (for state E during which dips occur), this implies nD^2 is $\sim 2 \times 10^{35}$ cm^{-1}. If we assume that the material causing the dips is at the outer edge of the accretion disk, calculated earlier to be at $\sim 3.2\ R_\odot$, then we obtain $n = 5 \times 10^{12}$ cm^{-3}. The ionization time scale at this radius is much shorter than the free-tall time. The Keplerian velocity at this distance from the source ($\sim 4 \times 10^7$ cm s^{-1}) and the duration of the dips (~ 700 s) imply that the diameter of a typical clump must be $\sim 3 \times 10^{10}$ cm, and its total column density $\sim 2 \times 10^{23}$ cm^{-2}. A problem with this model is that if oxygen is 99% ionized we should see an O VIII absorption edge near 14 Å. While we do see an absorption feature near 14 Å, it is too narrow to be an edge.

The analysis above assumes solar abundances. Another means for reducing the absorption for a given N_H is the lowering of metal abundances (White and Swank 1982). Since our high-resolution data do not give evidence for abundance anomalies, we favor an interpretation in terms of highly ionized matter.

The dips are probably related to the dips seen in systems such as Her X-1, MXB 1659−29, and 4U 1915−05 (Walter *et al.* 1982; White and Swank 1982; Cominsky and Wood 1984) which are thought to be caused by the interaction of the gas stream from Roche lobe overflow with the disk, resulting in gas streams projecting well above and below the disk (Lubov and Shu 1976; Flannery 1975). The dips observed in Cygnus X-2 are not as deep or as regular as those in Her X-1; this may be attributed to the fact that the inclination of Cyg X-2 is probably less than 70° (CCH), whereas the inclination of Her X-1 is around 90°. If matter at the disk edge flaring up is causing the dips, there will be less interference in systems with low inclinations than in systems that show actual eclipses.

VI. CONCLUSIONS

Cygnus X-2 is highly variable in both flux and spectral shape. All the observations are well fitted by single-temperature thermal bremsstrahlung (TB) models (with temperatures ranging from 4–12 keV in different states), as well as by several two-component (2BB, BB+TB, PL+TB) models. We favor the single-component TB model since it provides a good fit to the data with a minimum of free parameters, although no detailed physical picture that yields a pure TB spectrum for binary X-ray sources has been worked out. The highest temperature (12 keV) occurs during the lowest intensity state (A), and it is proposed that this is due to Compton heating of the thermal bremsstrahlung by a hot corona. The observed source temperature and previously estimated mass of the neutron star (CCH) yield a coronal radius of 0.1 $R_\odot$.

The irregular dips of up to 30% in intensity that last for 300–700 s and are seen only during the high state can be interpreted as clumps of accreting matter intercepting the line of sight at a radius of $\sim 3\ R_\odot$ (corresponding to the outer edge of the accretion disk). The observed increase in column density and the appearance of an absorption feature (attributed to Fe XVIII) at 14.3 Å, during the dips support this interpretation. The dips occur at a binary phase consistent with occultation by the accretion stream.

The previously noted high and low X-ray states of the system appear to be corerlated with the 9.843 day optical period. This correlation is probably a consequence of X-ray heating of V1341 Cyg by Cygnus X-2. The binary-phase dependence of this correlation can be interpreted as implying partial eclipsing of the X-ray source.

Our luminosity versus spectral hardness distribution shows a structure similar to that reported by Makishima and Mitsuda (1985) for a composite of several low-mass X-ray binaries, suggesting that the spectral hardness is primarily a function of luminosity and is independent of the detailed properties

of individual sources. We attribute the positive correlation at high luminosities to a simultaneous increase of column density with intensity. This may be due to changes in the accretion rate: increases in accretion rate cause both luminosity increases and add obscuring matter to the line of sight. The interpretation in terms of intervening accreting matter is supported by the observation of an absorption feature in the high-resolution spectra at the same (14.3 Å) position as during the dips.

In the high-state intervals for which OGS data are available, emission features are seen which can be attributed to highly ionized states of Fe, Ne, and O. This is the first spectroscopy of Cygnus X-2 in the soft X-ray band (0.2–1.5 keV) with resolution sufficient to detect line features. The identified features are consistent with those expected for a hot collisional plasma with temperature $T > 5 \times 10^6$ K. However, it should be noted that the circumsource medium responsible for these features may be photoionized rather than collisionally excited. The absorption line at 14.3 Å attributed to Fe XVIII, the only absorption feature seen, is probably caused by matter at the outer edge of the accretion disk.

We find that the tremendous spectral and temporal variability observed in Cygnus X-2 can be explained by a simple model of a soft thermal source with a variable rate of accretion surrounded by a hot corona. Simultaneous optical, ultraviolet, and X-ray observations would be of interest in view of the intriguing correlation found between the X-ray and *U*-band light curves.

S. D. V. would like to thank J. Halpern, J. Kylafis, J. McClintock, and R. Burg for stimulating discussions, and M. Rudenko, E. Bohlen, A. MacDonald, and D. Redmond for their help during the early stages of the data analysis. We would also like to acknowledge the extensive work on the OGS software done by Tomek Chelebowski. This work was supported in part by NASA grant NAG8-497. S. D. V. acknowledges support from ZONTA International through an Amelia Earhart Fellowship. This is Contribution No. 293 of the Columbia Astrophysics Laboratory.

REFERENCES

Bonnet-Bidaud, J. M., and van der Klis, M. 1982, *Astr. Ap.*, **116**, 232.
Bowyer, S., Byam, E. J., Chubb, T. A., and Friedmann, H. 1965, *Science*, **17**, 894.
Bradt, H. V. D., and McClintock, J. E. 1983, *Ann. Rev. Astr. Ap.*, **21**, 1.
Branduardi, G., Kylafis, N. D., Lamb, D. Q., and Mason, K. O. 1980, *Ap. J. (Letters)*, **235**, L153.
Branduardi-Raymont, G., Chiappetti, L., and Ercan, E. N. 1984, *Astr. Ap.*, **130**, 175.
Brinkman, A. C., Mewe, R., Langerwerf, T., Heise, J., Peacock, A., and White, N. 1985, *Space Sci. Rev.*, **40**, 201.
Chiappetti, L., Maraschi, L., Tanzi, E. G., and Treves, A. 1983, *Ap. J.*, **265**, 354.
Cominsky, L. R., and Wood, K. S. 1984, *Ap. J.*, **283**, 765.
Cowley, A. P., Crampton, D., and Hutchings, J. B. 1979, *Ap. J.*, **231**, 539.
Doschek, G. A., and Cowan, R. D. 1984, E. O. Hulburt Center for Space Research preprint.
Efron, B. 1982, *The Jackknife, the Bootstrap and Other Resampling Plans* (Bristol, England: Arrowsmith).
Flannery, B. P. 1975, *M.N.R.A.S.*, **170**, 325.
Gaillarditz, R., *et al.* 1979, *IEEE Trans. Nucl. Sci.*, **25**, 437.
Giaconni, R., Gorenstein, P., Gursky, H. H., Usher, P., Waters, J., Sandage, A., Osmer, P., and Jugaku, J. 1967, *Ap. J. (Letters)*, **148**, L129.
Gorenstein, P. 1975, *Ap. J.*, **198**, 95.
Grindlay, J. E., *et al.* 1980, *Ap. J. (Letters)*, **240**, L121.
Halpern, J. P. 1984, *Ap. J.*, **281**, 90.
Hasinger, G., Langmeier, A., Pietsch, W., and Sztajno, M. 1985*a*, MPE preprint No. 30.
Hasinger, G., Langmeier, A., Sztajno, M., Trumper, J., Lewin, W. H. G., and White, N. E. 1985*b*, MPE preprint No. 36.
Hatchett, S., Buff, J., and McCray, R. 1976, *Ap. J.*, **206**, 847.
Henry, J. P., *et al.* 1977, *Proc. SPIE*, **106**, 196.
Hirano, T., Hayakawa, S., Kuneida, H., Makino, F., Masai, K., Nagase, F., and Yamashita, K. 1984, *Pub. Astr. Soc. Japan*, **36**, 769.
Holt, S. S., Kaluzienski, L. J., Boldt, E. A., and Serlemitsos, P. J. 1979, *Ap. J.*, **233**, 344.
Iben, I., Jr., and Tutukov, A. V. 1984, *Ap. J.*, **284**, 719.
Ilovaisky, S. A., Chevalier, C., Motch, C. and Janot-Pacheco, E. 1979, *IAU Circ.*, No. 3325.
Kahn, S. M., and Grindlay, J. E. 1984, *Ap. J.*, **281**, 826.
Kahn, S. M., Seward, F. D., and Chlebowski, T. 1984, *Ap. J.*, **283**, 286.
Kallman, T. R., and McCray, R. 1982, *Ap. J. Suppl.*, **50**, 263.
Kellogg, E., Baldwin, J. R., and Koch, D. 1975, *Ap. J.*, **199**, 299.
Kylafis, N. D., and Lamb, D. Q. 1982, *Ap. J. (Letters)*, **48**, 239.
Lewin, W. H. G., and van Parajdis, J. 1985, preprint.
Lubov, S., and Shu, F. 1976, *Ap. J.*, **198**, 383.
Makishima, K., and Mitsuda, K. 1985, in *Proc. Japan–US Seminar on Galactic and Extragalactic Compact X-Ray Sources*, ed. Y. Tanaka and W. H. G. Lewin (Tokyo: Institute of Space and Astronautical Science), p. 127.
Marshall, N., and Watson, M. G. 1979, *IAU Circ.*, No. 3318.
McClintock, J. E., Petro, L. D., Hammerschlag-Hansberge, G., Proffitt, C. R., and Remillard, R. A. 1984, *Ap. J.*, **282**, 794.
Morrison, R., and McCammon, D. 1983, *Ap. J.*, **270**, 119.
Pravdo, S. H. 1983, *Ap. J.*, **270**, 239.
Ryter, C., Cesarsky, C. J., and Adouze, J. 1975, *Ap. J.*, **198**, 103.
Seward, F. D., *et al.* 1982, *Appl. Optics*, **21**, 2012.
Swank, J. H., and Serlemitsos, P. J. 1985, in *Proc. Japan–US Seminar on Galactic and Extragalactic Compact X-Ray Sources*, ed. Y. Tanaka and W. H. G. Lewin (Tokyo: Institute of Space and Astronautical Science), p. 175.
Walter, F. M., Bowyer, S., Mason, K. O., Clarke, T. T., Henry, J. P., Halpern, J. P., and Grindlay, J. E. 1982, *Ap. J. (Letters)*, **53**, L67.
White, N. E., and Holt, S. S. 1982, *Ap. J.*, **257**, 318.
White, N. E., Peacock, A., Hasinger, G., Mason, K. O., Manzo, G., Taylor, B. G., and Branduardi-Raymont, G. 1985, EXOSAT preprint No. 14.
White, N. E., and Swank, J. H. 1982, *Ap. J. (Letters)*, **253**, L61.

J. E. GRINDLAY and F. D. SEWARD: Harvard-Smithsonian Center for Astrophysics, 60 Garden Street, Cambridge, Ma 02138

D. J. HELFAND: Columbia Astrophysics Laboratory, Columbia University, 538 West 120th Street, New York, NY 10027

S. M. KAHN: Department of Physics, University of California, Berkeley, CA 94720

S. D. VRTILEK: Code 666, NASA/Goddard Space Flight Center, Greenbelt, MD 20771